CO_x-free hydrogen production from ammonia at low temperature using Co/SiC catalyst: Effect of promoter

M. Pinzón, A. Romero, A. de Lucas-Consuegra, A.R. de la Osa, P. Sánchez*.

Chemical Engineering Department, Faculty of Chemical Sciences and Technology, University of Castilla-La Mancha, Avda. Camilo José Cela 12, 13071 Ciudad Real, Spain.

*Corresponding author:

e-mail address: Paula.Sanchez@uclm.es

Abstract

Cobalt catalysts (5 wt.%) using β-SiC as a support and modified with different alkaline (K and Cs), alkaline-earth (Ca and Mg) and rare-earth (La and Ce) metals were prepared, characterized, and examined in the hydrogen production from ammonia decomposition at low temperatures. Porous SiC has been proved to be a suitable support for promoted cobalt catalysts, which are highly active for the target decomposition reaction. Catalysts modified with small amount (1 wt.%) of K and La remarkably enhanced the catalytic activity whereas the addition of Cs, Mg, Ca or Ce to cobalt catalyst decreased the ammonia conversion with respect to the unpromoted catalyst. The total basic sites and electron-donor properties of the K metal modified the electronic structure of cobalt active sites increasing the ammonia conversion at low temperatures. However, an excess of K promoter resulted in a decrease in the hydrogen production due to the blockage of the active sites. Therefore, the catalyst containing 1 wt.% K and 5 wt.% Co resulted in an excellent H_2 production associated with an ammonia conversion close to 100 % at 450 ºC. Moreover, the selected catalyst provided suitable performance stability after one day of reaction.

Keywords

Ammonia decomposition, hydrogen production, silicon carbide, cobalt, promoters.

1. Introduction

The future of energy sector needs of the substitution of conventional technologies for power generation with the use of carbon-free energy sources. The exploitation of clean, sustainable and renewable energy sources is essential for a transition towards the elimination of greenhouse gas emission of energy generation processes [1]. Hydrogen (H_2) generation from renewable sources seems to be a potential alternative, using fuel cells and internal combustion engines by releasing only water such as by-products [2–4]. However, H_2 has low volumetric energy density, which increases storage and transport cost [5]. Therefore, successful hydrogen storage procedures are essential to distribute large quantities of renewable energy.

In this sense, safe and economical H_2 storage and transport could be carried out by using hydrogen-rich molecules ('hydrogen carries') which present well-established technologies of production and distribution [6]. These could be decomposed in situ into hydrogen through suitable conversion processes [7]. Ammonia is considered a promising hydrogen carrier due to its excellent properties [1,3–6] and, it can storage energy in long-term compared to battery systems (short-term storage) [8]. Moreover, its decomposition only produced hydrogen and nitrogen. In other words, NH_3 is an exceptional carbon-free hydrogen vector [9].

To release H_2 contained in NH_3 for power generation it is necessary to reduce the ammonia in the outlet stream. High purity H_2 (99.97%) is essential to be used in PEMFC (proton exchange membrane fuel cells) and other technology such as AFC (alkaline fuel cells) allows an inlet stream with a 9 % of ammonia concentrations [10,11]. Hence, a robust, efficient, and economic active catalyst at low temperature, and a separation unit to separate H_2 from N_2 and unconverted NH_3 is required. Thus, the thermodynamic equilibrium could be achieved increasing the hydrogen purity and, decreasing the energy cost of the process [10,12].

Auspicious results of H_2 generation from NH_3 at low temperatures are achieved with ruthenium catalysts [13–15]. Moreover, other factors clearly influence the catalytic activity such as the support and the use of proper electron-donor promoters [16–18]. Regarding the catalytic support, those with the best properties for this reaction must have high electron conductivity, basicity, and thermal stability, as well as the absence of electron-withdrawing species [19]. Porous silicon carbide (β-SiC) possesses suitable physicochemical properties to be used as catalytic support: a high resistance, high thermal conductivity and, chemical inertness. Indeed, a homogeneous temperature distribution within the catalyst bed could be achieved by its high thermal conductivity, suitable for ammonia decomposition reaction. To the date, interesting results have been reached in multiple catalytic reactions using silicon carbide as catalytic support [13,20–22]. In this sense, our previous results demonstrated the exceptional activity on ammonia decomposition reaction over ruthenium supported on SiC catalyst, achieving an ammonia conversion close to 100% at 350 ºC [13]. Nevertheless, ruthenium is a limited and expensive metal, which makes it difficult to use on an industrial scale. Non-noble metals, mainly nickel (Ni) and cobalt (Co), are considered economic active phase for catalysts due to their high catalytic activity in NH_3 decomposition, availability, and low cost. Although Co-based catalysts leads higher ammonia conversion than Ni-based ones [23,24], it is necessary to improve their catalytic activity and stability [25].

Recently, different promoters have been studied to improve the ammonia decomposition reaction through the increase of the electron density in the metal by increasing of the basic sites of the catalysts [23,26,27]. Additionally, it is known that the addition of promoters to non-noble metals catalysts could modify the metal particle size increasing the metal dispersion, maintaining the stability of the catalyst over long reaction times by the inhibition of the agglomeration of metal particles [23,26].

In the present work, Co supported on novel β-SiC has been studied for the first time as catalyst for H_2 generation by NH_3 decomposition reaction. The influence of different promoters (alkaline, alkaline-earth and rare-earth metals) and the promoter loading on the catalytic performance was analysed in detail.

2. Experimental

2.1 Catalyst preparation

Alkaline (K and Cs), alkaline-earth (Mg and Ca) and rare-earth (La and Ce)-modified cobalt-supported β-SiC catalysts were prepared by the vacuum co-impregnation method using an aqueous solution of cobalt nitrate $Co(NO_3)_2 \cdot 6H_2O$ (Panreac) as precursor, to give a final catalyst with 5 wt.% cobalt and, the corresponding amount of nitrate salts to obtain 1 wt.% of metal promoter (K, Cs, Mg, Ca, La and Ce), and 0.5 wt.% and 1.5 wt.% of K promoter. β-SiC (25 $m^2 \cdot g^{-1}$ and 14.1 $cm^3 \cdot g^{-1}$, Sicat Catalysts) structured as pellets (3 mm length and 1 mm diameter) was used as the catalyst support. First, 1.5 g of support was pre-treated under vacuum at 80 ºC for 2 h, using a rotatory evaporator. Later, an aqueous solution of the cobalt and the promoter precursors was incorporated drop by drop over the pellets. After each impregnation, the catalysts were dried under vacuum at 80 ºC to remove the solution (repeated three times). Finally, the catalysts were dried at 100 ºC overnight and subsequently calcined at 500 ºC for 1 h (10 ºC·min^{-1}) under N_2 flow (50 mL·min^{-1}). Samples were denoted as *yM-Co/SiC (M=K, Cs, Mg, Ca, La and Ce)*, where *y* represented nominal promoter loading (wt.%).

2.2 Catalysts characterization

Co metal content was determined by Inductively Coupled Plasma Atomic Emission Spectroscopy (ICP-AES) on a Varian Liberty RL Sequential equipment. Samples were

dissolved in 3 mL of hydrofluoric acid, 2 mL of hydrochloric and 2 mL of hydrogen peroxide followed by microwave digestion (250 ºC). Textural properties (surface area, S_{BET}, and pore volume, V_p) of samples were calculated from N_2 adsorption-desorption isotherm at -196 ºC using a QUADRASORB 3SI sorptometer apparatus. The multi-point BET method was used to determine the S_{BET} and the total pore volume was calculated at relative pressure of $P/P_0 = 0.99$. Prior to analysis, samples were outgassed at 180 ºC in gross vacuum ($6.6 \cdot 10^{-9}$ bar) for 4 h. X-ray Powder Diffraction (XRD) experiment were conducted with a Philips X'Pert MPD instrument using co-filtered Cu-Kα radiation (λ=1.54056 Å). Samples were scanned at a rate of 0.02º ·step^{-1} from 2θ=10-80º with a scan time 2 s·step^{-1}. Scherrer equation was used to determine the metallic Co size assuming the particle were spherical [28]. High Resolution Transmission Electron Microscopy (HRTEM) analysis were carried out in a TalosTM F200X (FEI) equipment working at 200 kV. The particle sizes distribution was estimated by HRTEM images, evaluated as the surface-area weighted diameter and was calculated according to procedure explained elsewhere [13]. More than 200 particles were measured for each material showing a Gaussian particle distribution. Elemental mapping was also carried out with an energy dispersive X-ray spectrometer (EDX, X-Max Oxford) provided with 4 X-ray detectors and a X-FEG beam.

Sample reducibility was studied by H_2 temperature-programmed reduction (H_2-TPR). Analysis was carried out in a commercial Micromeritics AutoChem 2950 HP equipment with a TCD detector. Each catalyst (0.12 g) was outgassed by heating at 20 ºC·min^{-1} in Ar flow up (50 mL·min^{-1}) to 250 ºC. After cooling to room temperature and stabilized under a 5 v/v% H_2/Ar mixed gas (60 mL·min^{-1}). Then, the sample was heating at 900 ºC (10 ºC·min^{-1}). In order to get information related to the basic sites of the catalysts, CO_2 temperature programmed desorption (CO_2-TPD) was carried out in the same equipment

as used in TPR analysis. First, 0.1g of calcined sample was reduced by a 5 v/v% H_2/Ar gas flow (60 mL·min^{-1}) at a heating rate of 10 ºC·min^{-1} to 550 ºC. After cooling to 50 ºC in an Ar flow (20 mL·min^{-1}), the sample was exposed to a CO_2 flow (40 mL·min^{-1}) at 50 ºC for 30 min, and then replaced by Ar (20 mL·min^{-1}) for 1h. Finally, the sample was heated at 10 ºC·min^{-1} to 900 ºC.

X-Ray photoelectron spectroscopy (XPS) measurements were performed using an ultrahigh vacuum (UHV) multipurpose surface analysis system Specs, equipped with a Phoibos 150-MCD energy detector, with Al Kα X-ray source (1486.6 eV) in 'stop and go' mode. Deconvolution of experimental curves was done with Gaussian and Lorentzian line fitting, minimizing the χ^2 values.

2.3 Catalytic activity measurements

Catalytic ammonia decomposition tests were carried out in a fixed-bed quartz reactor, with a fritted quartz plate located in the middle (10 mm i.d. and 50 mm of length), at atmospheric pressure at a gas hourly space velocity (GHSV) of 60000 mL·g_{cat}^{-1}·h^{-1}, operating at a 250 to 450 ºC temperature range. The reactor was placed in a furnace (*Hornos Electricos A.T.*) equipped with a temperature-programmed system and the temperature of the catalysts bed was measured with a K-type thermocouple (Thermocoax). Calibrated mass flow meters (Brooks 5850 E) were used to control the gas flows and reaction gases were Air Liquide certified standards (H_2, 99.999%, N_2, 99.999%, Ar, 99.999% and NH_3, 5.000% of purity). All the pipes were heated at 70 ºC to prevent any ammonia condensation and, in turn, corrosion.

The amount of catalyst used in the experiments was 0.1 g in pellets form. Prior to reaction, the catalysts were reduced with a 50 v/v% H_2/Ar flow (100 mL·min^{-1}) at 400 ºC (for alkaline and rare-earth promoted catalysts) and 550 ºC (for alkaline-earth promoted catalysts) for 1 h (heating rate 10 ºC·min^{-1}). After cooling to 250 ºC with a flow of Ar

(100 mL·min^{-1}), a 5 v/v% NH_3 stream (100 mL·min^{-1}) was fed into the reactor. Reaction products were analysed on-line by using a gas chromatograph (Agilent 7820A) composed of two parallel columns (CP Molsieve 5 Å and CP-PoraBond Q) connected to a thermal conductivity detector (TCD) using argon as the carrier gas. Therefore, the hydrogen formation rate (mmol H_2·min^{-1}·g_{cat}^{-1}) was calculated from the H_2 content in the outgas stream, while NH_3 (X_{NH_3}) conversion was calculated as follows: $X_{NH_3}(\%) = (F_{NH_{3_{in}}} - F_{NH_{3_{out}}}/F_{NH_{3_{in}}})\cdot 100$, where $F_{NH_{3_{in}}}$ and $F_{NH_{3_{out}}}$ referred to the inlet and outlet NH_3 molar flows (mmol gas·min^{-1}), respectively. Note that, the ammonia conversion was also calculated considering the molar expansion of the reaction [29,30]. The ammonia conversion was very similar showing a relative error lower than 0.8 %.

Furthermore, apparent activation energy of the synthesized catalysts was calculated from the Arrhenius plot at low conversion values (<20%), assuming that the reaction was carried out into differential conditions. Moreover, for the experimental condition studied here, the reaction is not limited by equilibrium [29,30].

In addition, the turnover frequency (TOF, h^{-1}) was calculated according to the equation [31]: $TOF(h^{-1}) = (r_{H_2}(mmolH_2\cdot g_{Co}^{-1}\cdot h^{-1})\cdot A_{Co}(g_{Co}\cdot mol^{-1}))/(D/100)$, where r_{H_2} is the formation rate of hydrogen, A_{Co} is the atomic mass of Co (58.93 g_{Co}·mol^{-1}), and D (%) is the cobalt dispersion.

Note that the data provided in this research corresponds to the average of three consecutive measurements once the reaction stabilised at the desired temperature. Ammonia conversion with the blank reactor and β-SiC support was negligible under the operating conditions.

At the last stage, the stability of selected catalysts for ammonia decomposition was tested at 400 ºC over 24 hours.

3. Results

3.1. Influence of different metal promoters

An exhaustive evaluation of six different metal promoters (K, Cs, Mg, Ca, La and Ce) with a load of 1 wt.% in 5 wt.% Co supported on β-SiC for ammonia decomposition reaction has been carried out.

All catalysts were successfully synthesized by the vacuum co-impregnation method [32]. Cobalt content (error of ±1%) and textural properties of the support, unpromoted (Co/SiC) and promoted catalysts are shown in **Table 1**. N_2 adsorption-desorption isotherms are shown in **Figure S1** of the Supporting Information.

Table 1. Cobalt content and textural properties catalysts.

Sample	Co content (%)	S_{BET} ($m^2 \cdot g^{-1}$)	V_p ($cm^3 \cdot g^{-1}$)
SiC	-	25	0.14
Co/SiC	5.2	24	0.10
1K-Co/SiC	4.1	19	0.14
1Cs-Co/SiC	4.7	17	0.16
1Ca-Co/SiC	4.1	29	0.16
1Mg-Co/SiC	4.2	30	0.13
1La-Co/SiC	4.1	24	0.14
1Ce-Co/SiC	4.5	24	0.11

The catalysts exhibited type II isotherms, according to the IUPAC classification, which is characteristic of non-porous or macroporous materials [33]. Moreover, the H3-type hysteresis loop observed at high relative pressure is attributed with capillary condensation [22]. All samples showed isotherms similar to of the support, which indicated that the β-SiC surface did not change after metal impregnation [22]. In fact, the S_{BET} of promoted catalysts was similar to that of the unpromoted one [34]. The slight variation observed between catalysts was due to the experimental measurements error (±5%) [22]. Moreover, it is important to note that upon the co-impregnation with promoters metals the surface

area might decreased compared to that of the support, suggesting a partial blockage of the β-SiC pores [35,36]. In conclusion, it can be said that, regardless of the type of promoter, its incorporation into the catalyst does not significantly affect the textural properties.

The crystalline structure of the promoted catalysts before reduction was studied by XRD and showed in **Figure 1**. The XRD results for the support and Co/SiC catalyst before reduction are shown in **Figure S2**.

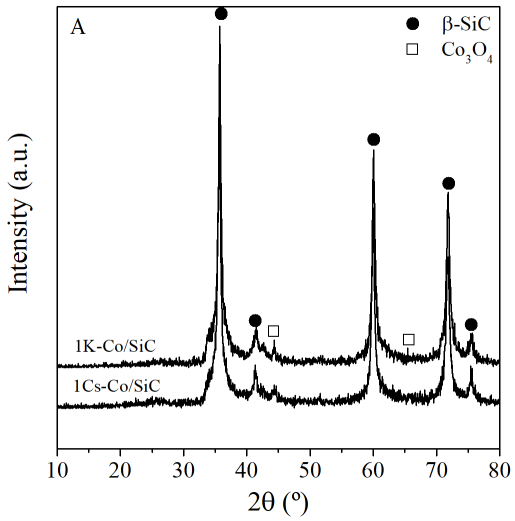

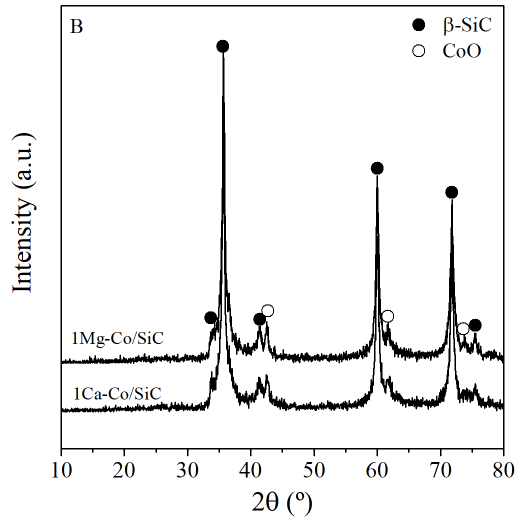

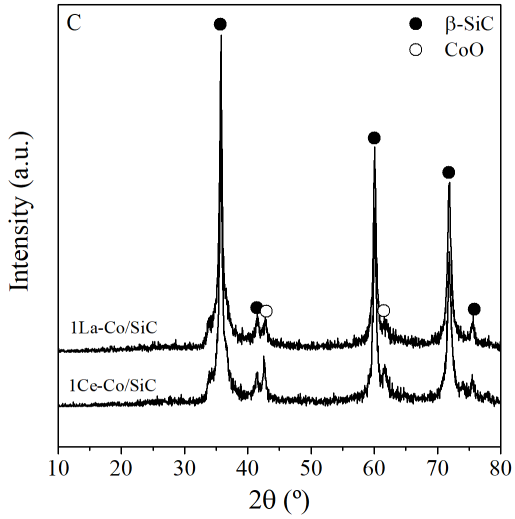

Figure 1. XRD patterns for A: alkaline, B: alkaline-earth and C: rare-earth promoted catalysts before reduction.

The catalyst without promoters showed the main reflections related to β-SiC support (JCPDS: 02-1050), peaks at 2θ (hkl) = 31.2º (2 2 0), 36.8º (3 1 1), 44.8º (4 0 0) and 65.2º (4 4 0) corresponding to cubic Co_3O_4 (JCPDS: 42-1467), and peaks at 2θ (hkl) = 42.3º (2 0 0) and 61.5º (2 2 0) ascribed to cubic CoO (JCPDS: 48-1719) [35]. All promoted catalysts showed the β-SiC structure. Obviously amorphous SiO_2 should be present, but the α-cristobalite phase could be seen after addition of promoters and subsequent calcination at high temperature [21]. This means that the 1 wt.% loading of promoters did not poison the SiC support and inhibit its oxidation to α-cristobalite. The diffraction pattern for the alkaline (K and Cs) promoted catalysts before reduction is shown in **Figure 1A**. These catalysts also showed peaks at 2θ (hkl) = 44.6º (4 0 0) related to cubic Co_3O_4 (JCPDS: 42-1467) [37]. **Figure 1B** and **1C** showed the XRD patterns of the alkaline-earth (Mg and Ca) and rare-earth (La and Ce) promoted cobalt-based catalysts, respectively. Peaks at 2θ (hkl) = 42.5º (2 0 0) and 61.7 º (2 2 0) associated with cubic cobalt oxide (CoO) (JCPDS: 48-1719) were observed. The XRD data suggested, that cobalt species on alkaline-earth and rare-earth promoted catalysts were moderately

reduced to CoO by interaction with the promoters and silicon carbide support after calcination under nitrogen atmosphere [38]. No peaks associated to alkaline, alkaline-earth and rare-earth oxides were detected, indicating that their particle sizes were very small being highly dispersed on the support or that, the amount of metal precursors was very low to by detected by XRD [37,39]. In addition, if the amount of the metal oxides were higher, they would interact with the silica, presented in SiC surface, leading to metal silicates [40]. Based on the literature [37,41], metal promoters increased the particle size of cobalt oxide species favouring their reduction. To check it, the crystal size of CoO and Co_3O_4 particles was calculated using Scherrer equation at $2\theta = 42.5^o$ and 44.2^o for CoO and Co_3O_4, respectively (**Table 2**). It was observed that, in general, the particles size of the different cobalt oxide species increased with the addition of promoters. The largest particle size was observed on rare-earth promoted catalyst (1La-Co/SiC and 1Ce-Co/SiC) with an average particle size of 21.7 nm and 21.6 nm, respectively. Taking into account that the average pore size of β-SiC support was 10 nm (**Table 1**), it can be stated that the CoO and Co_3O_4 would be located on the external surface of the support [35]. Thus, the cobalt reduction over promoted catalysts might be carry out at lower temperatures than the unpromoted catalyst [37].

Table 2. Particle size, dispersion, total basic sites and H_2 consumption of unpromoted and promoted catalysts.

Sample	XRD-Particle diameter (nm)		TEM-Particle diameter (nm)	Co dispersion[b] (%)	Total basic sites (mmolCO_2·g_{cat}^{-1})[c]	H_2 consumption (mmolH_2 g_{cat}^{-1})
	CoO[a] (2θ=42.5º)	Co_3O_4[a] (2θ=44.2º)				
Co/SiC	12.7	12.8	10.3	9.3	0.015	1.5
1K-Co/SiC	-	19.8	10.2	9.4	0.059	1.2
1Cs-Co/SiC	-	12.1	10.4	9.2	0.043	1.7
1Ca-Co/SiC	19.9	-	13.7	7.0	0.022	1.9
1Mg-Co/SiC	14.5	-	8.8	10.1	0.020	1.4
1La-Co/SiC	21.7	-	10.9	8.8	0.038	1.9
1Ce-Co/SiC	21.6	-	11.3	8.5	0.039	1.9

[a]Calculated by Scherrer equation.

[b]Calculated by [37].
[c]Calculated from the reduced catalysts at 400 ºC.

In order to analyse the effect of the promoters on the cobalt reducibility, H_2-TPR experiments were carried out of the promoted catalysts (**Figure 2**). Note that H_2-TPR profiles of the support and the non-promoted catalyst are also plotted in **Figure S3** for comparison purposes. Firstly, there were not any peaks associated with the SiC support, indicating that all hydrogen consumption peaks in the profiles were related to changes in cobalt species. In agreement with previous works [37,38,41,42], the unpromoted catalyst gave rise two H_2 consumption peaks at 307 ºC and 349 ºC associated to the reduction of Co_3O_4 to CoO and CoO to Co^0. As observed, the alkaline promoted catalysts presented similar TPR profiles (**Figure 2A**). 1K-Co/SiC catalyst exhibited two main reduction peaks at 257 ºC and 345 ºC and 1Cs-Co/SiC catalyst showed two peaks at around 269 and 334 ºC, related to the cobalt oxide species reduction to metallic cobalt. It can be observed that the first peak ascribed to the Co_3O_4 to CoO reduction was shifted to lower reduction temperatures (about 50 ºC in 1K-Co/SiC and, 40 ºC in 1Cs-Co/SiC) compared to the unpromoted catalyst, which has been related to the higher particle size of Co_3O_4 observed on XRD analysis (**Figure 1**) [37]. In the case of alkaline-earth promoted catalysts, a different TPR trend was observed (**Figure 2B**). Ca promoted catalyst showed peaks at 291 and 358 ºC and, Mg promoted catalyst at 268 ºC, 432 ºC and 666 ºC. Low temperatures peaks were ascribed to the reduction of cobalt species to Co^0. The high temperature peak (666 ºC) has been attributed to the reduction of CoO species with a strong interaction with the β-SiC support, which is promoted by magnesium [23,24,43]. All reduction peaks were associated with cobalt species reduction, since TG and DTG analysis of alkaline-earth nitrate salts previously carried out in our research group [37] exhibited that their decomposition take place at temperatures lower than 500 ºC. Finally, the rare-earth promoted catalysts also exhibited two main reduction peaks at 296 ºC and

383 ºC for La promoted catalyst and peaks at 283 ºC and 373 ºC for Ce promoted catalyst, ascribed to the metal oxides reduction [43]. In this sense, the addition of different promoters may cause soft changes in the reduction behaviour of the cobalt-based catalysts. However, the H_2 consumption (**Table 2**) during TPR analysis showed that Co was reduced independently of promoter ions, since all catalysts exhibited similar H_2 consumption. Moreover, the reduction degree of unpromoted and promoted catalysts was estimated from the ratio of the real H_2 consumption to the theoretical amount of H_2 required for the complete reduction of Co_3O_4, and it was around 65%.

Bearing in mind the TPR results, the conditions for in situ reduction at 400 ºC for alkaline and rare-earth promoted catalysts and 550 ºC for alkaline-earth in 50 v/v% H_2-Ar flow ensured the most of Cobalt reduction and the formation of Co^0, which is considered the active phase for hydrogen generation from ammonia.

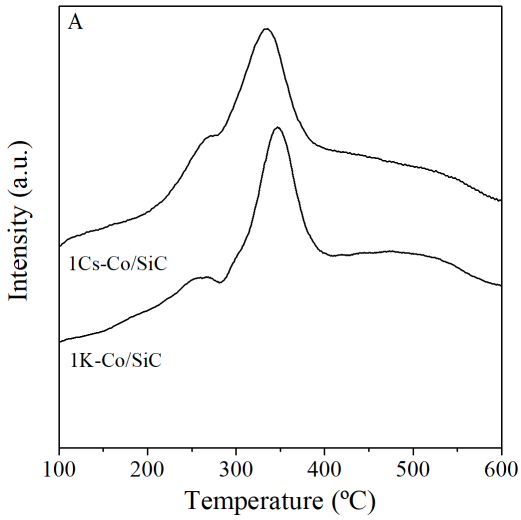

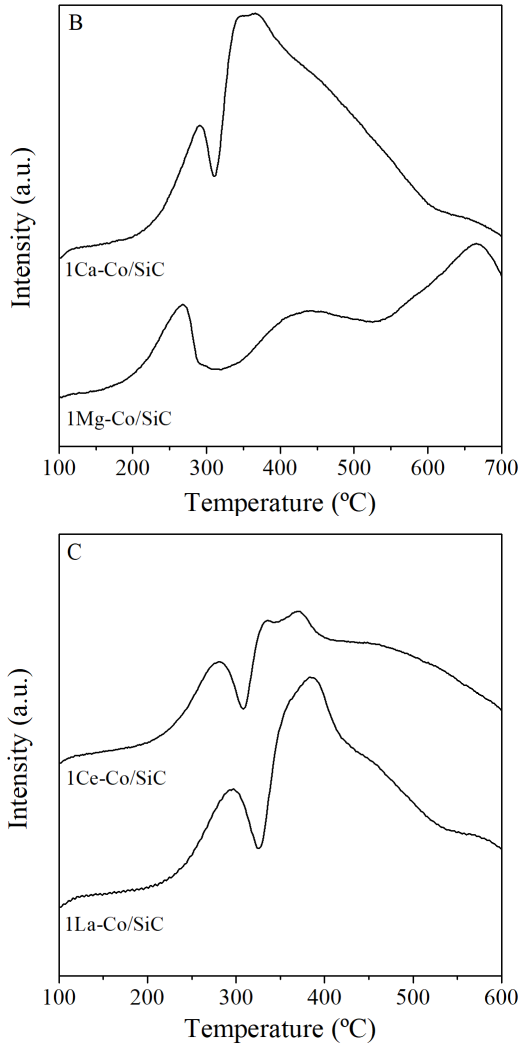

Figure 2. H_2-TPR curves for A: alkaline, B: alkaline-earth and C: rare-earth promoted catalysts.

It is generally accepted that the active site for ammonia decomposition reaction is metallic cobalt [18]. Therefore, in order to corroborate the presence of metallic Co^0 over the promoted catalysts after the reduction treatment, XRD measurements were carried out. **Figure 3** showed the XRD patterns of reduced catalysts. The reduced unpromoted catalyst presented the main peaks related to the support (β-SiC), as well as a peak at 2θ= 44.3 º attributed to the formed cubic metallic cobalt phase (JCPDS: 15-0806) [44]. The promoted cobalt-based catalysts showed the same crystal phases as the unpromoted one and the cubic metallic cobalt phase, indicating that the reduction treatments were adequate to reduce cobalt species and obtain the Co active sites. Alkaline-earth promoted

catalysts, which were reduced at 550 º C, showed cubic metallic cobalt phase, which indicated that the reduction temperature was enough to reduce cobalt species and even those with strong metal-support interaction, in agreement with H_2-TPR results. Moreover, the intensity of the peak associated with metallic cobalt was similar, which suggested that the metallic cobalt particle sizes were not greatly affected by promoters. This tendency has also been observed by other authors [45].

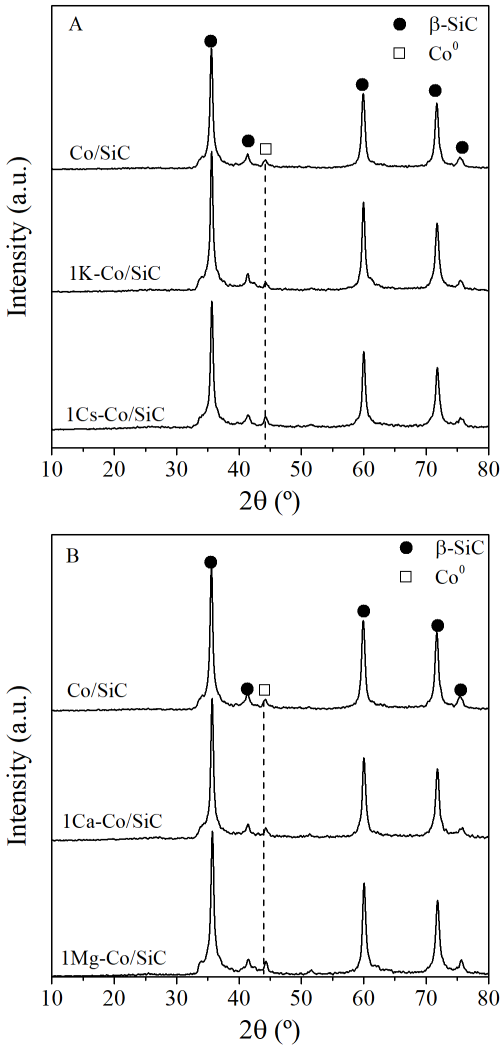

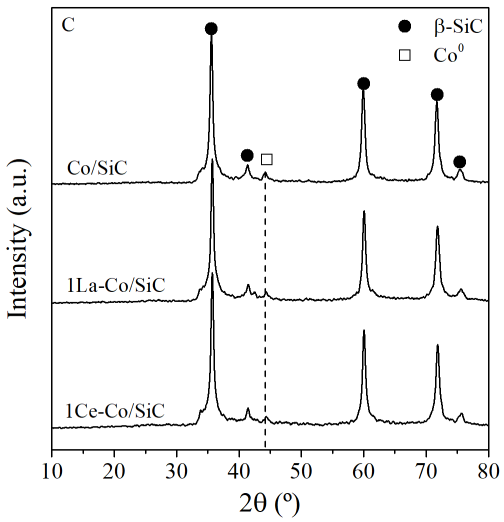

Figure 3. XRD patterns for A: alkaline, B: alkaline-earth and C: rare-earth promoted catalysts after reduction.

Once the catalysts were characterized by XRD, TEM images of reduced catalysts were performed in order to obtain information about the distribution and size of the cobalt particles. For comparative purposes, a TEM image, the particle sizes distribution and EDX elemental mapping of the unpromoted catalyst are shown in **Figure S4**. The unpromoted catalyst showed well-dispersed nanosized cobalt particles of hemispherical shape with an average size of 10.3 nm. **Figure 4A, 4B** and **4C** shows the TEM images and particle size distribution of the different promoted catalysts. As the unpromoted catalyst, all promoted ones exhibited a Gaussian particle size distribution with an average relative error of around ± 0.3 nm. The mean particle size evaluated by TEM and the cobalt dispersion are shown in **Table 2**. As expected, promoted catalysts showed similar metallic cobalt particle sizes than that of the unpromoted catalyst, indicating not an influence of promoter ions on metal particle sizes and dispersion [45], in good agreement with XRD results of the reduced catalysts. Elemental mapping (**Figure S5**) confirmed the presence of cobalt, silica, carbon, alkaline (K or Cs), alkaline-earth (Mg or Ca) and rare-earth (La or Ce) over the different reduced promoted catalysts, while no impurities were found. Note that, both promoters and cobalt particles were well-dispersed over the support despite its low specific surface area and pore volume (25 $m^2 \cdot g^{-1}$ and 0.14 $cm^3 \cdot g^{-1}$,

respectively) except for the 1Ca-Co/SiC catalyst, where calcium was agglomerated and not well dispersed, as can be seen by EDX maps of 1Ca-Co/SiC. Regardless of the promoter used, the particle size distribution and dispersion obtained after reduction were similar for all catalytic systems. Based on the obtained characterisation results and previous ones [13] it can be confirmed that β-SiC support is suitable for the preparation of electron-donor promoted Co catalysts.

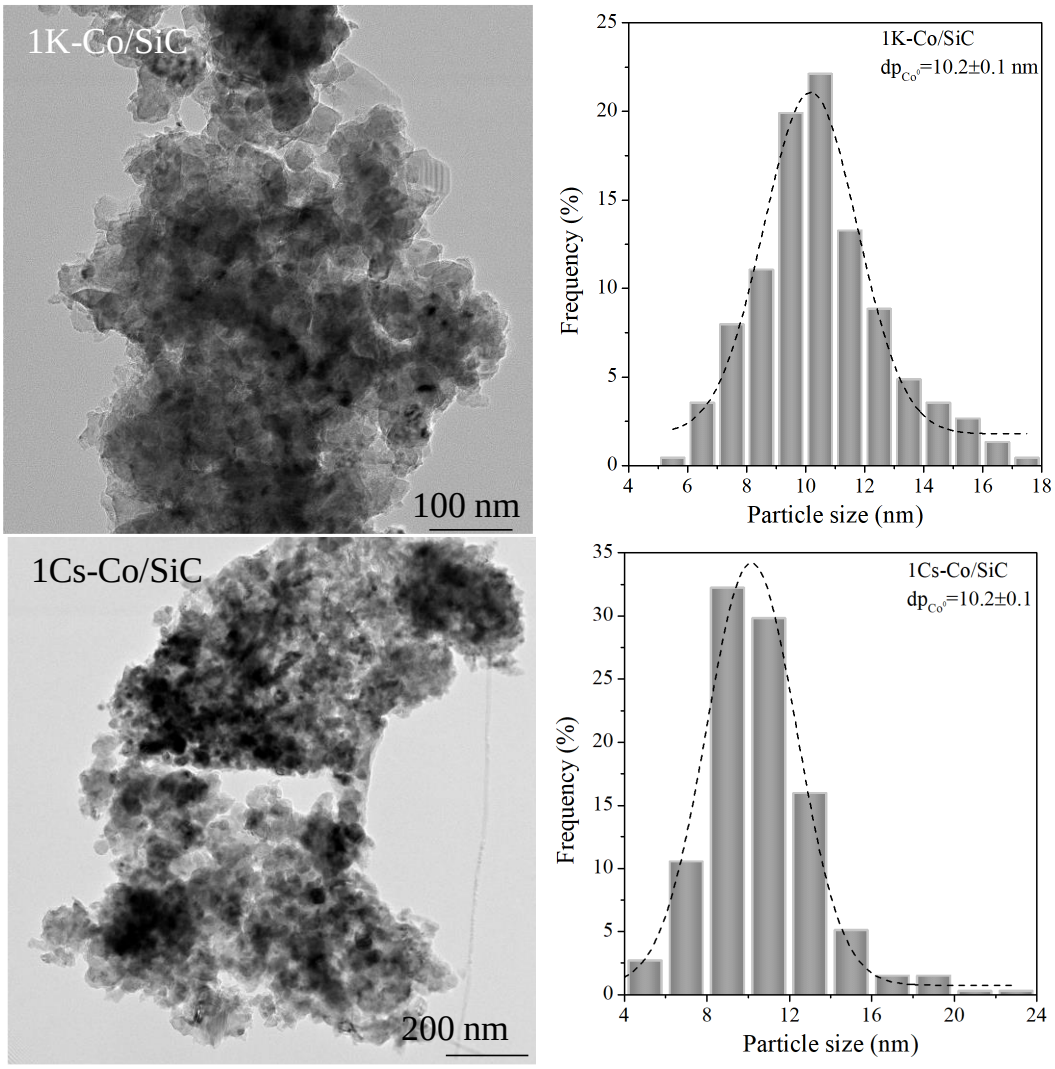

Figure 4A. TEM images and particle sizes distribution of reduced alkaline promoted catalysts.

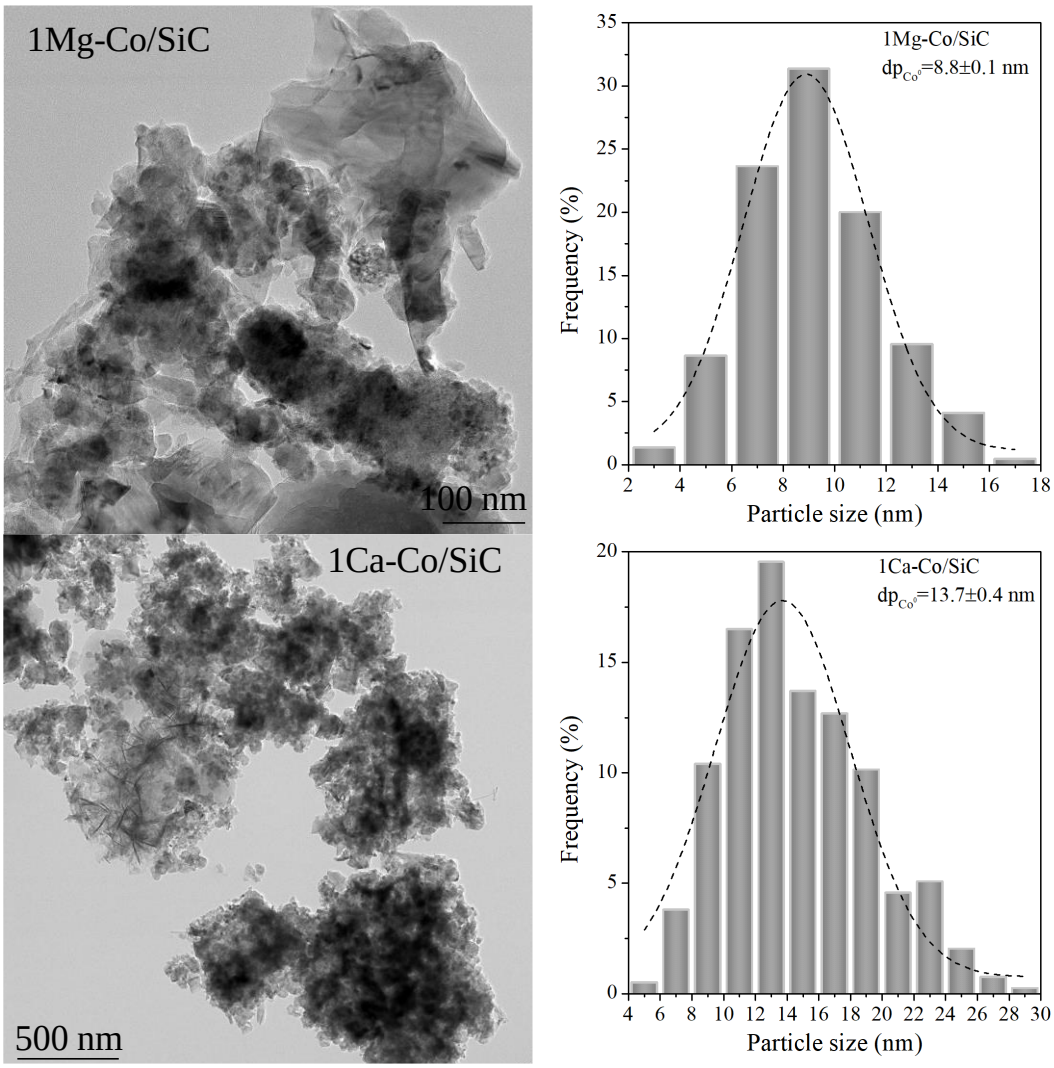

Figure 4B. TEM images and particle sizes distribution of reduced alkaline-earth promoted catalysts.

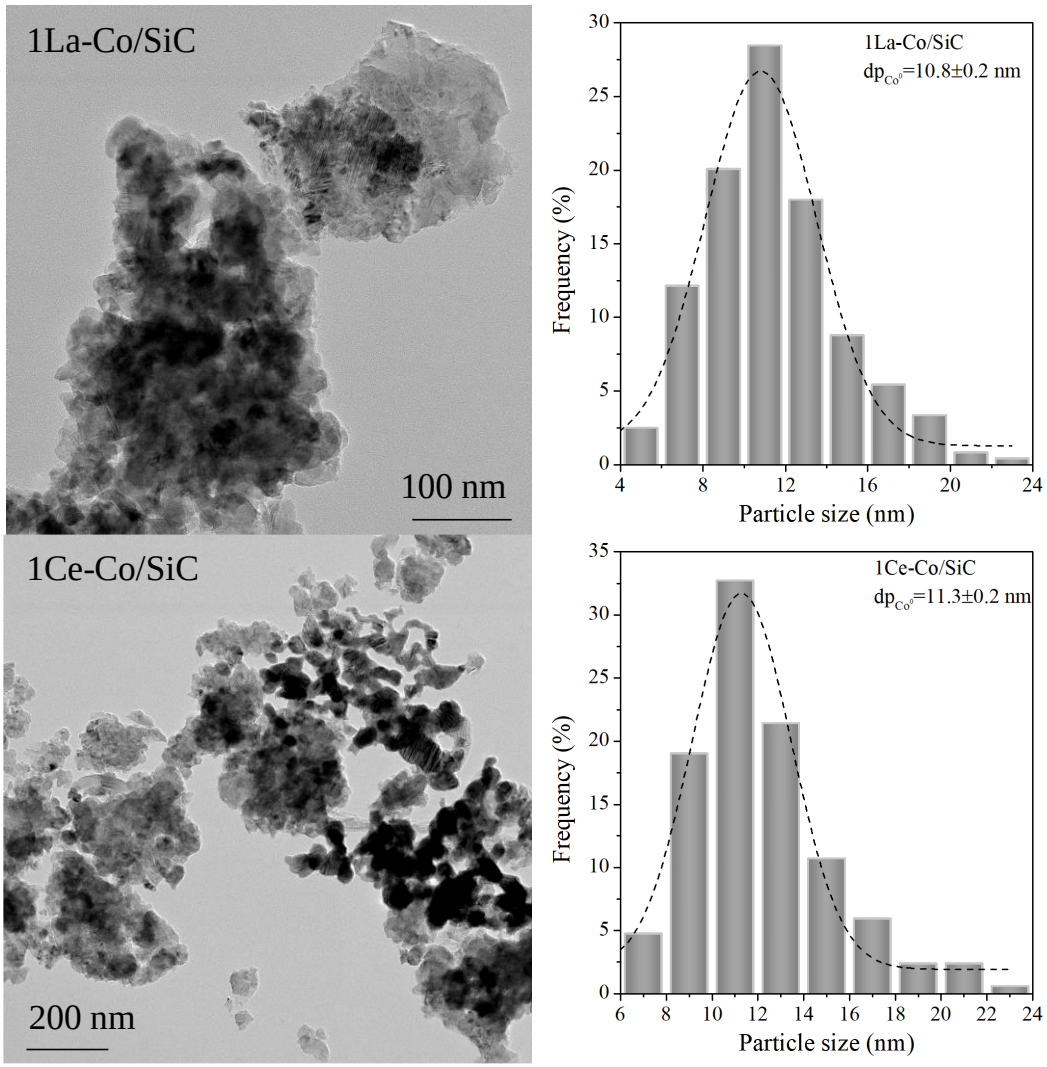

Figure 4C. TEM images and particle sizes distribution of reduced rare-earth promoted catalysts.

It is well known that the addition of promoter can modify the basic properties of the catalysts. In this sense, CO_2-TPD experiments were carried out over reduced unpromoted and promoted catalysts. **Figure 5** exhibits the CO_2-TPD curves of the support, reduced unpromoted and promoted catalysts. Both the temperature and peak integration was used to determine the strength and quantity of the basic sites on the catalyst surface [43,46]. It is known that, β-SiC support did not influence on the basic properties [47,48] with a relative amount of CO_2 desorbed at high temperature 0.017 mmol$CO_2 \cdot g_{cat}^{-1}$. The addition of cobalt in low amount into the support did not seem to modify its basic properties, and a small desorption peak was only observed at high temperatures, which corresponded to

0.015 mmol$CO_2 \cdot g_{cat}^{-1}$ total basic sites. It was in agreement to that reported elsewhere showing that the addition of low amount of non-noble metals such as nickel or cobalt on β-SiC support did not slightly changed the relative basicity (~0.01 mmol$CO_2 \cdot g_{cat}^{-1}$) [35,48,49]. On the other hand, the addition of the proposed promoter ions increased the basic properties (see the total amount of desorbed CO_2 in **Table 2**) of the catalysts which has been widely studied for other reactions [37,46]. First, the alkaline promoted samples displayed different desorption peaks at low and high temperatures. The soft peak at 90 ºC was related to weakly adsorbed CO_2 on the surface whereas the higher temperature (T>500 ºC) desorption region was associated with strongly adsorbed CO_2 on the surface. In the case of alkaline-earth promoted catalysts, three desorption regions at temperatures i) 100-200 ºC, ii) 200-500 ºC and iii) >500 ºC were clearly observed. These regions may be explained by CO_2 interaction with weak, moderate and strong basic sites [37,43]. Finally, the incorporation of rare-earth metals to the cobalt-based catalyst also showed three desorption regions in the same temperature ranges [43]. All promoted catalysts showed higher total amount of desorbed CO_2 than the unpromoted catalyst, which could increase the catalytic activity for ammonia decomposition reaction. Among them, catalysts with a lower amount of basic sites were the alkaline-earth promoted ones (1Mg-Co/SiC and 1Ca-Co/SiC). However, the alkaline metals, in particular 1K-Co/SiC, exhibited the highest amount of basic sites (0.059 mmol$CO_2 \cdot g_{cat}^{-1}$), which was expected to further promote the catalytic reaction.

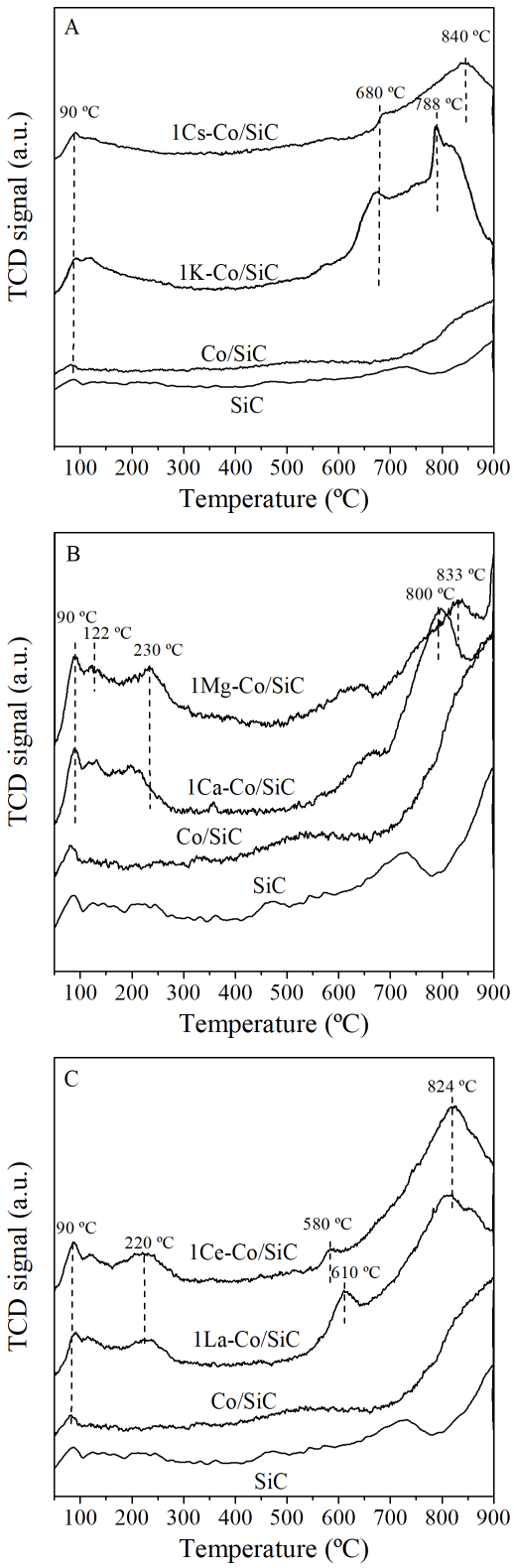

Figure 5. CO_2-TPD profiles of A: alkaline, B: alkaline-earth and C: rare-earth promoted catalysts after reduction.

In order to determine the influence of the physicochemical properties on the intrinsic activity of the promoted catalysts, the TOF value (at 350 ºC), the hydrogen formation rate

(at 350 ºC) and, the apparent activation energy (E_a, calculated from the Arrhenius plot) of each catalyst were calculated and showed on **Table 3**.

Table 3. Ammonia conversion, hydrogen formation rate, TOF values and apparent activation energy of the catalysts at 350 ºC.

Sample	NH_3 conversion (%)	TOF (s^{-1})	H_2 formation rate ($mmolH_2 \cdot g_{Co}^{-1} \cdot min^{-1}$)	E_a ($kJ \cdot mol^{-1}$)
Co/SiC	27.2 ± 0.2	0.19 ± 0.1	18.6 ± 0.1	104.2 ± 0.3
1K-Co/SiC	33.1 ± 0.3	0.23 ± 0.1	24.9 ± 0.2	97.5 ± 0.4
1Cs-Co/SiC	25.2 ± 0.4	0.17 ± 0.1	19.5 ± 0.2	107.2 ± 0.0
1Ca-Co/SiC	4.8 ± 0.2	0.01 ± 0.0	5.3 ± 0.1	117.3 ± 1.7
1Mg-Co/SiC	24.9 ± 0.2	0.15 ± 0.0	18.1 ± 0.0	104.8 ± 0.4
1La-Co/SiC	27.4 ± 0.1	0.20 ± 0.0	20.1 ± 0.1	101.4 ± 0.3
1Ce-Co/SiC	20.4 ± 0.3	0.16 ± 0.1	14.6 ± 0.2	113.9 ± 2.1

It can be seen that not all the promoted catalysts enhanced the intrinsic activity of the unpromoted catalyst (7.1 h^{-1}). Alkaline promoted catalysts showed TOF values of 9.3 (1K-Co/SiC) and 7.1 h^{-1} (1Cs-Co/SiC) which is in agreement with other results showing that the addition of K to the cobalt catalyst increased the ammonia conversion [50,51], but Cs led to a decrease in the catalytic activity as occurs when this promoter is added to cobalt supported on carbon materials [42]. The differences in the intrinsic activity cannot be attributed to different metal particle sizes, according to the obtained TEM results (**Table 2**), but to the higher increase number of basic sites with the addition of K metal. Alkaline-earth promoted catalysts clearly showed a detrimental effect on ammonia decomposition reaction. Note that, these two materials not only showed different cobalt particle sizes (13.7 nm for 1Ca-Co/SiC and 8.8 nm for 1Mg-Co/SiC), which in turn modified the catalytic activity, but also provided the lowest amount of basic sites among all promoted catalysts. By the way, in the available literature Ca and Mg have been reported to be suitable promoters for non-noble catalysts in hydrogen production from

ammonia [52]. However, the addition of these metals into ruthenium catalyst led to lower ammonia conversion that the unpromoted catalyst. Likewise, in this work both alkaline-earth metals resulted in cobalt catalysts with lower intrinsic activity that the unpromoted catalyst, specially 1Ca-Co/SiC catalyst, which can be explained by the worst calcium dispersion and the highest cobalt particle size. In the case of 1Mg-Co/SiC catalyst, magnesium might modify the active sites and show lower capacity to desorb nitrogen easily (which is considered the rate determining step in the ammonia decomposition reaction), thus, resulting in a lower activity than that of the unpromoted one [52]. Finally, regarding rare-earth promoted catalysts, 1La-Co/SiC reached a higher TOF value (8.0 h^{-1}), whereas the 1Ce-Co/SiC showed a slightly lower catalytic performance than that of the unpromoted catalyst. The higher lanthanum promoted effect in comparison with cerium over cobalt-based catalysts has been extensively described by some authors [23,43,53,54], being related to its high electron-donor effect and its ability to inhibit the metal agglomeration. Moreover, cobalt and nickel catalysts doped with lanthanum supported on magnesium oxide have been reported to enhance both the adsorption and decomposition of ammonia and the nitrogen desorption step [23]. However, the lower TOF values of 1Ce-Co/SiC catalyst might be related to the higher inhibition effect of hydrogen on Ce in comparison with La in non-noble catalysts, which was observed by *Okura et al.* [54].

Summarizing, some authors have recently suggested that an increase in the TOF values of promoted catalysts could be related to an alteration in the electronic structure of the metal active sites by the addition of promoter metals [51,55]. In agreement with this, both the highest basicity of the 1K-Co/SiC catalyst and changes in the electronic structure of cobalt active sites improved the catalytic activity.

The same trend observed for the TOF was found for hydrogen production rate and the apparent activation energy (E_a) values, achieving the 1K-Co/SiC catalyst the highest

hydrogen formation rate at lower temperature. It was related to the lowest E_a and the suitable properties above mentioned, whereas the 1Ca-Co/SiC catalyst showed the lowest hydrogen formation rate, which was associated the lowest basic sites available, and the highest cobalt particle size observed by TEM. The apparent activation energy determined for the unpromoted and promoted cobalt catalysts was in the range of E_a previously reported for cobalt-based catalysts [23,24,42,56,57].

As above mentioned, the ammonia decomposition reaction should be optimized to achieve high ammonia conversion (high hydrogen production) at low temperatures, in order to reduce the energy requirements and enhance the ammonia perspective as hydrogen carrier toward the 'hydrogen economy'. The ammonia conversion evolution versus reaction temperature of the unpromoted and promoted catalysts is plotted in **Figure 6**. As observed, the ammonia conversion of cobalt-based catalysts was clearly altered by the addition of alkaline, alkaline-earth and rare-earth promoter metals. In this sense, the addition of alkaline metals (**Figure 6A**) improved the ammonia conversion at lower temperatures, showing the 1K-Co/SiC catalysts the highest ammonia conversion i.e. 33.1 % and hydrogen formation rate (24.9 $mmolH_2 \cdot g_{Co}^{-1} \cdot min^{-1}$) at 350 ºC, which could be related to the highest basicity of this material and the electronic structure alteration of the active sites induced by potassium. In agreement, the apparent activation energy (**Table 3**) of this catalyst was the lowest among all the promoted catalysts as it was also obtained by other authors using Ru as metal active phase [58]. Alkaline-earth promoted catalysts (**Figure 6B**) did not improve the ammonia conversion in a larger extension at low temperature compared with the unpromoted catalyst, which might be due to the undesirable properties of these catalysts, above mentioned. Similar results have been obtained by different authors in which the addition of alkaline-earth metals as promoters decreased the catalytic activity vs. the unpromoted catalysts [36]. Regarding rare-earth promoted catalysts, 1La-Co/SiC reached a similar (27.3 % for) ammonia

conversion than the unpromoted catalyst at 350 ºC while a decrease of its value to 20.4% was obtained when 1Ce-Co/SiC was used, which can be due to the physicochemical characteristics previously discussed.

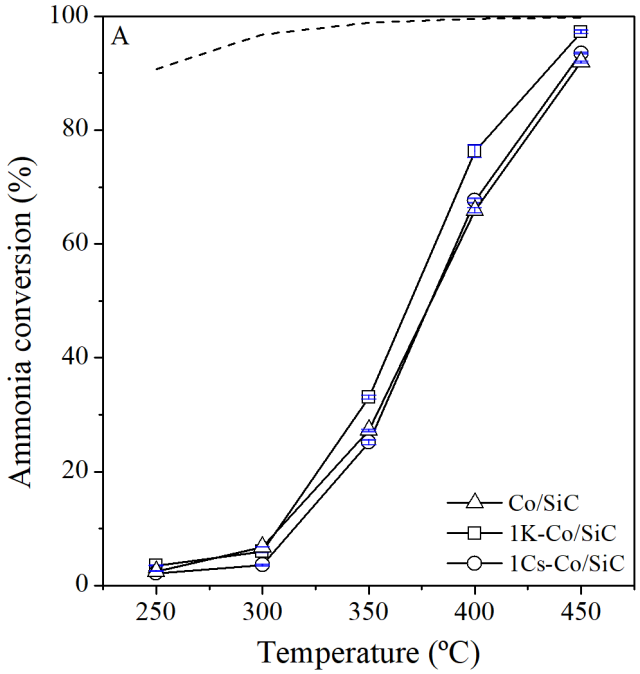

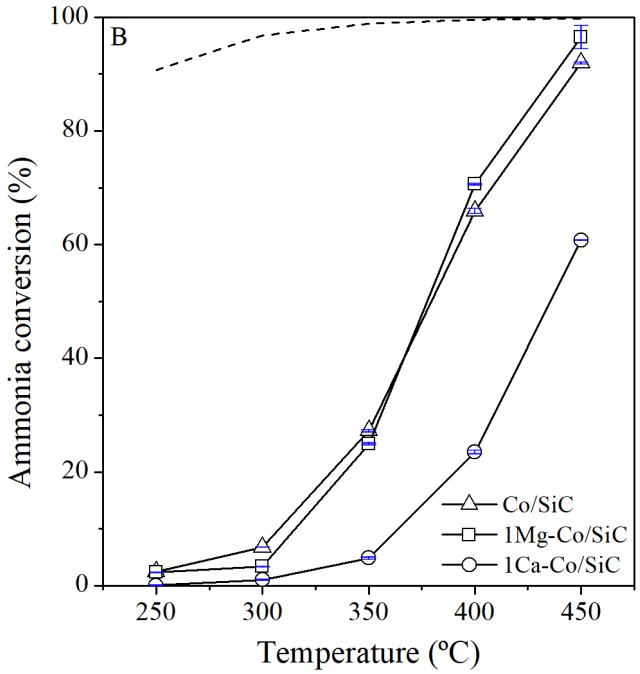

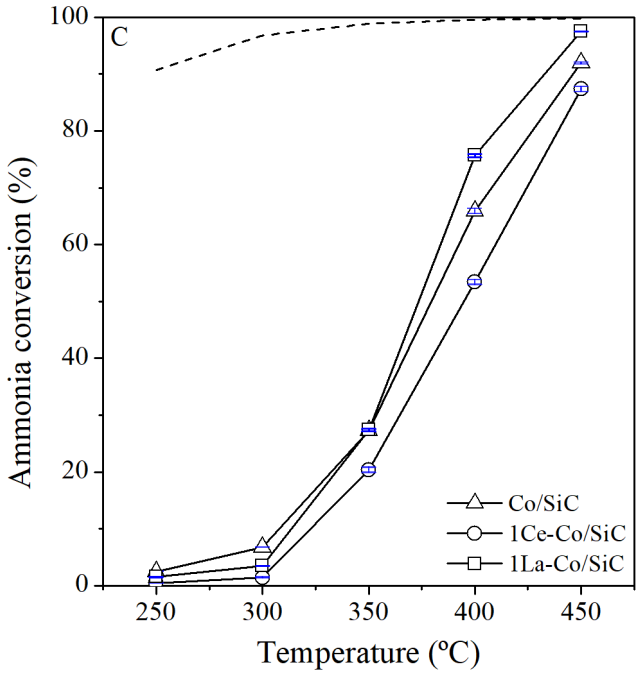

Figure 6. NH_3 conversion of A: alkaline, B: alkaline-earth and C: rare-earth promoted catalysts. Dash line represents the equilibrium conversion at atmospheric pressure [59].

Usually, the promoting effect of promoter metals on the catalytic activity of Co, Ni and Ru catalysts is clarified by their capacity to donate electrons to the metal surface, which is established on the results of X-ray photoelectron spectroscopy (XPS) [60–62]. In this sense, XPS analysis of the unpromoted, potassium and lanthanum promoted catalysts were carried out and showed in **Figure 7**. Note that, the cobalt spectra presented the Co $2p_{3/2}$ and $Co2p_{1/2}$ peaks appearing because of a spin-orbital splitting (15.2 eV) and the two satellites structure of these peaks [63]. For the unpromoted catalyst maximum peak of 2p region of Co species appeared at 782.93 eV characteristic of cobalt supported on SiC [63]. However, after the addition of promoters (K and La), this peak shifted toward lower binding energy (BE), at 782.57 eV and 782.63 eV for 1K-Co/SiC and 1La-Co/SiC catalysts, respectively. Many authors suggested that the displacement of metal peaks to lower BE values side by the addition of promoters was a consequence of a change in the electronic state of the metal [60,61]. This phenomenon occurred by the transfer of electrons from the promoter metals to the cobalt. Moreover, a higher displacement toward

smaller BE values indicated higher electron-donation effect [62]. For that reason, XPS analysis suggested that potassium promoted catalysts showed higher electron-donation than that of lanthanum for cobalt supported on SiC, enhancing the ammonia decomposition reaction.

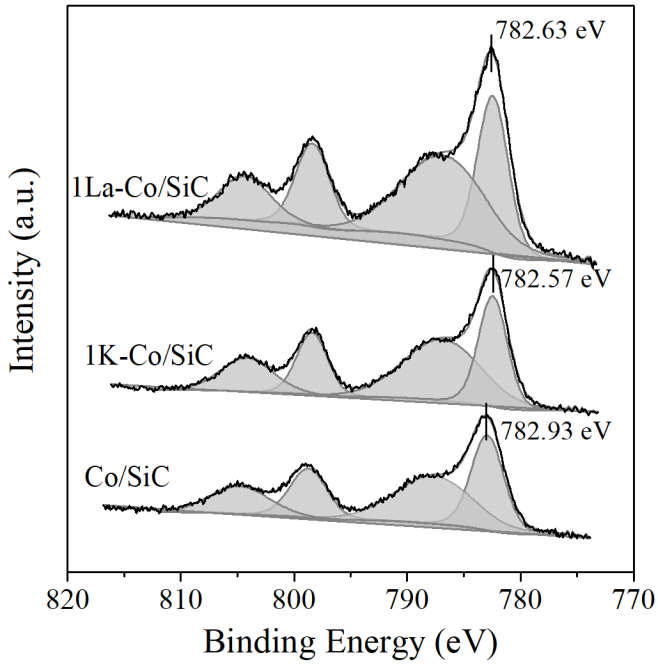

Figure 7. Co 2p core level spectra of reduced unpromoted, 1K-Co/SiC and 1La-Co/SiC catalysts.

Anyway, alkaline (K) and rare-earth (La) promoted cobalt catalysts showed excellent intrinsic activity for hydrogen production by ammonia decomposition reaction due to their adequate physicochemical properties. However, the ammonia conversion of 1La-Co/SiC was similar than that unpromoted catalysts and the electron-donor properties was lower than potassium promoted catalyst. The size of the metal particles did not significantly influence on the catalytic activity of the promoted catalysts whereas, the total basic sites, the electron-donor properties and the electronic structure changes of cobalt active site induced by K are key to increase it at low temperatures. Taking into

account the obtained results, the K promoted catalyst was selected to carry out the following study.

3.2. Influence of potassium metal (K) loading

In order to better understand the influence of the potassium loading on the catalytic hydrogen production performance, three different loadings (0.5, 1 and 1.5 wt.%) were co-impregnated with 5 wt.% cobalt over β-SiC support.

All potassium promoted catalysts exhibited a cobalt content around 5 wt.%, which indicated that the vacuum co-impregnation method is an efficient procedure to synthesize promoted cobalt-based catalyst over porous silicon carbide. Surface area (S_{BET}) and pore volume (V_p) of promoted catalysts calcined at 500 ºC are shown in **Table S1**. It could be observed that the potassium loading had not a remarkable influence on the textural properties; all materials showed lower surface area than that of the support maybe due to the partial blockage of the pores of the support after cobalt and potassium impregnation [36,44]. In addition, the N_2 adsorption-desorption isotherms are shown in **Figure S6**. Isotherms did not change with the potassium loading showing type II isotherms with H3-type hysteresis loop (according to the IUPAC classification). Hence, it can be stated that the textural properties of *y*K-Co/SiC catalysts calcined at 500 ºC are not significantly affected by the amount of potassium.

X-ray diffractograms of the calcined *y*K-Co/SiC catalysts (**Figure S7**) displayed the above-mentioned characteristic peaks of silicon carbide, and reflections at 2θ = 42.7º and 2θ = 44.6º related to the (2 0 0) and (4 0 0) planes of the cubic CoO and Co_3O_4, respectively. Note that, regardless of the potassium loading, no differences in the intensity of the peaks associated with the cobalt species were observed, neither were potassium

oxide peaks detected, suggesting that these species were either well-dispersed on the support or in such low amounts that could not be distinguished [64].

On the other hand, temperature-programme reduction (H_2-TPR) was used to investigate the effect of potassium loading on the reduction behaviour of the catalysts. As shown in **Figure S8**, the reduction process of the catalyst occurred in two stages, associated with the Co^{3+} to Co^{2+} and Co^{2+} to Co^0 reduction steps. The first reduction step was slightly modified by the potassium loading. It can be observed that the reduction temperature associated with Co_3O_4 to CoO reduction was shifted to lower temperatures as the potassium content increased [61]. This could be due to the interaction between the potassium species and cobalt oxide, which enhanced the first reduction step. The second reduction step, which was associated with the CoO to metallic cobalt reduction step, took place at temperatures around 350 ºC for three catalysts. In agreement with *Asano et al.* [61], the increase of potassium loading widen this peak which is related to cobalt species strongly interacting with the support [46]. To gain insight into the impact of the potassium loading on the cobalt reducibility, the H_2 consumption was estimated form the TPR results (**Table S1**). The H_2 consumption decreased with the increase of potassium, which suggest that the cobalt species strongly interacting with the support were hardly reduced. Therefore, the reduction degree diminished as the amount of K increased [46]. In this sense, potassium species seemed to play an important role in the cobalt reduction.

From the TPR results the reduction temperature for the ammonia decomposition tests was set at 400 ºC (using a 50 v/v% H_2-Ar flow) for all yK-Co/SiC catalysts, which assures that most of cobalt is maintained in its metallic form prior to reaction.

Considering this, the crystalline structure of the promoted catalysts after reduction at 400 ºC in hydrogen flow was studied by XRD (**Figure 8**). The reduced *y*K-Co/SiC catalysts showed the main peaks associated with the support (silicon carbide), as well as a peak at 2θ=44.3º related to the (1 1 1) plane of the cubic metallic cobalt (JCPDS: 15-0806). The

formation of Co^0 revealed that the selected reduction conditions before the ammonia decomposition reaction were suitable to get the metal active phase, and even to reduce the cobalt species in strong interaction with the support. No peak related to potassium species was appreciated indicating that they were highly well-dispersed over the catalysts. The cobalt particle size was determined by the Scherrer equation at peak 2θ=44.3 º (1 1 1) and shown in **Table S1**. It should be mentioned that the Scherrer equation method presents some limitations for quantitative purposes, but it is helpful for comparative ones [28]. As observed, although slightly modified [42], Co^0 particle size seemed to increase with the K loadings.

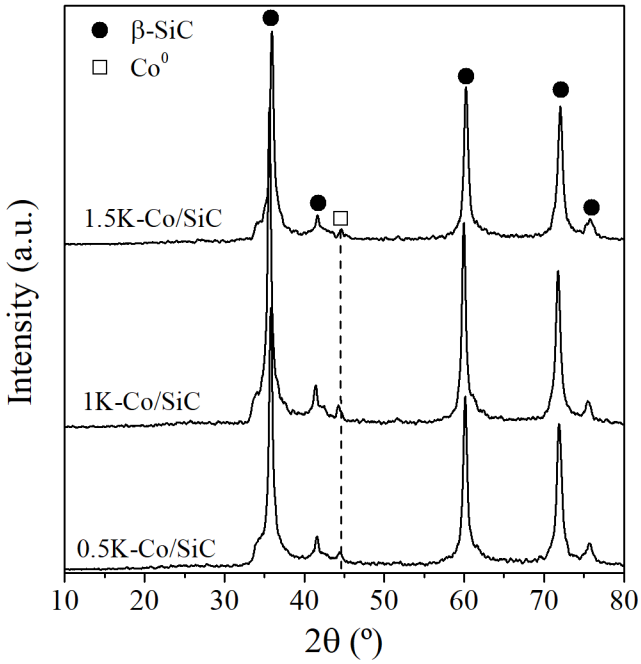

Figure 8. XRD patterns for the reduced *y*K-Co/SiC catalysts.

As demonstrated before, the basic properties seemed to have an important effect on catalytic activity of promoted cobalt catalysts. For that reason, the influence of potassium loading on the basicity of the catalysts was investigated. In this sense, temperature-programme desorption of CO_2 of the reduced catalysts are shown in **Figure 9** and the total basic sites are shown in **Table S1**. The potassium promoted catalysts exhibited two

desorption regions at i) 50-200 ºC and ii) > 500 ºC. Typically, peaks at lower temperatures (<200 ºC) are associated to weakly adsorbed CO_2 on the surface, whereas peaks at high temperatures (>500 ºC) are linked to strong basic sites. Note that the total amount of desorbed CO_2 was 0.053, 0.059 and 0.072 mmol $CO_2 \cdot g_{cat}^{-1}$ for 0.5, 1 and 1.5 wt.% cobalt catalysts, respectively, i.e., the basicity increased with the potassium content. As expected, the potassium loading modified the strength and total basic sites of the cobalt catalysts [46].

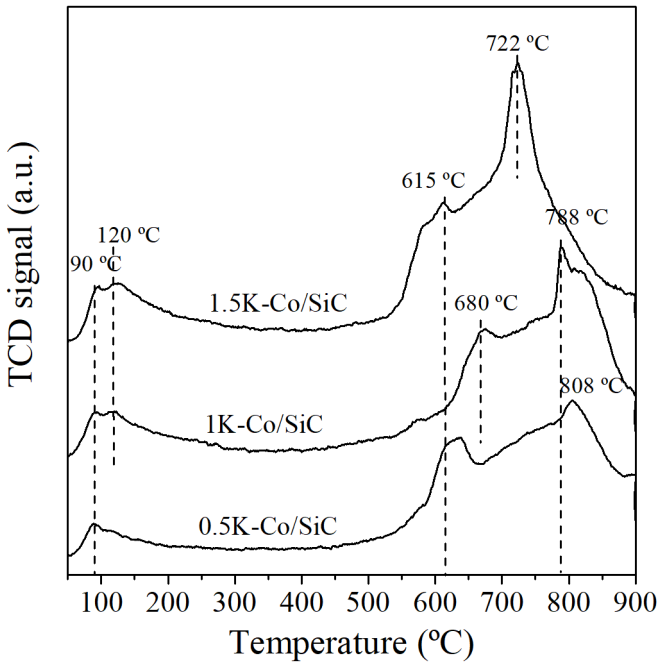

Figure 9. CO_2-TPD desorption profiles for the reduced *y*K-Co/SiC catalysts.

Once the *y*K-Co/SiC catalysts have been characterized, the effect of potassium loading on the catalytic performance was also studied. **Figure 10** shows the ammonia conversion evolution with the reaction temperature. As observed, the addition of potassium resulted in a higher ammonia conversion regardless of the potassium loading. As above mentioned, the electronic structure alteration produced by potassium increased the catalytic activity [36,51]. Note that, the ammonia conversion was very similar for 0.5 and 1 wt.% of potassium loadings for the whole temperature range. However, the catalytic

activity slightly decreased when the potassium loading was increased up to 1.5 wt.% due to an excess of potassium on the catalyst surface that can block the active sites and lower reduction degree of cobalt [36,65]. Similar results were obtained using Ru as the active phase [36]. Therefore, the optimum K loading was 1 wt.% which resulted in an ammonia conversion of 33.1 % at 350 ºC and the highest hydrogen formation rate (24.9 $mmolH_2 \cdot g_{Co}^{-1} \cdot min^{-1}$), at such temperature.

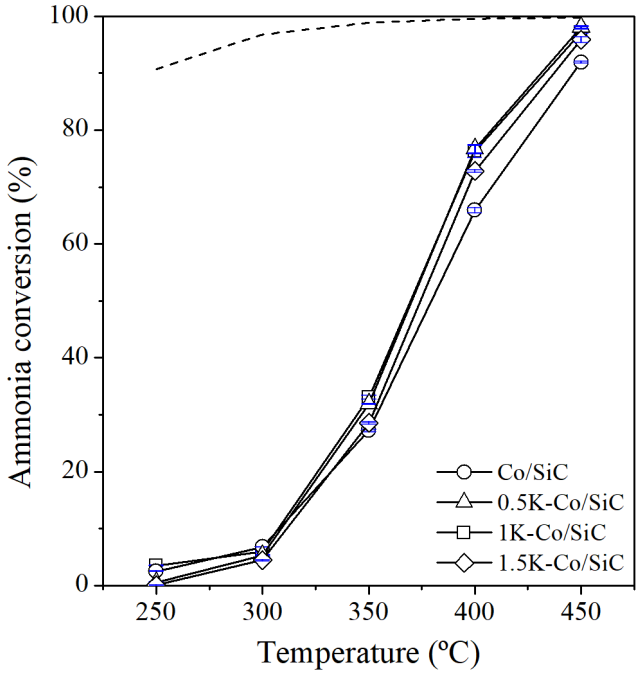

Figure 10. NH_3 conversion of *y*K-Co/SiC catalysts. Dash line represents the equilibrium conversion at atmospheric pressure [59].

Table 4 shows the hydrogen production rate and the apparent activation energy values determined from the Arrhenius plot of each potassium promoted catalysts. The obtained E_a, which was in the range of those previously obtained for cobalt catalysts [42,66], varied from 104.2 $kJ \cdot mol^{-1}$ (unpromoted catalyst) to 97.5 $kJ \cdot mol^{-1}$ (0.5K-Co/SiC and 1K-Co/SiC catalysts). This decrease in the apparent E_a is in good agreement with the good properties of the above-mentioned potassium promoted catalysts, which showed lower metal particle sizes and suitable basicity. The higher value of the apparent activation energy

was obtained with 1.5K-Co/SiC, which could be due to blockage of active sites which occurs above certain amount of promoter [36].

Also, the catalytic activity for the ammonia decomposition reaction of different catalysts studied in this work was compared with those obtained using different cobalt-base catalysts in other studies. The comparative was valued for similar high GHSV values and gas composition feed since it is well known that the ammonia conversion decreases as GHSV increases [17,24,51]. Noticeably, the *y*K-Co/SiC catalysts showed the highest catalytic activity at a lower temperature and similar reaction conditions due to their optimal characteristics: i.e., a high basicity, suitable electron-donor properties, and electronic structural changes of cobalt active sites on silicon carbide support due to the potassium promoter effect. Note that, a high hydrogen formation rate was observed for cobalt catalysts under pure ammonia feed stream but at high reaction temperatures (>500 ºC), which might increase the energy requirements for the ammonia decomposition application as hydrogen carrier toward the 'hydrogen economy'.

Table 4. Comparison of catalytic activity of *y*K-Co/SiC catalysts in the ammonia decomposition reaction at 450 ºC and at atmospheric pressure.

Catalysts	**GHSV ($mL \cdot g_{cat}^{-1} \cdot h^{-1}$)**	**NH_3 conversion (%)**	**H_2 formation rate ($mmolH_2 \cdot g_{Co}^{-1} \cdot min^{-1}$)**	**E_a ($kJ \cdot mol^{-1}$)**	**Ref.**
Co/SiC	60000 (5v/v%NH_3-Ar)	91.9	61.6	104.2	This work
0.5K-Co/SiC		98.1	65.7	97.2	
1K-Co/SiC		97.3	69.3	97.5	
1.5K-Co/SiC		95.9	64.2	102.0	
7.7Co/γAl_2O_3-imp	6000 (2.6v/v%NH_3-He)	11	0.5	99.1	[57]
14CoNaTi-NT	6000 (30v/v%NH_3-He)	4	59.5	89	[66]
7Co-AX-21	5200 (Pure NH_3)	25	20.7	89	[42]
7CoCs-AX-21		3	2.5	-	
20Co/La-MgO	22000 (Pure NH_3)	90[a]	117[a]	167	[23]
90Co/Al	72000 (Pure NH_3)	89[b]	79.5[b]	123	[24]

[a]Calculated at 500 ºC.
[b]Calculated at 600 ºC.

Finally, in order to check the stability behaviour of the optimally promoted catalyst (1K-Co/SiC), a durability test was carried out at 400 ºC, over 24 h, with a high GHSV of 60000 $mL \cdot g_{cat}^{-1} \cdot h^{-1}$ and a 5 v/v% ammonia feed stream (**Figure S9**). For comparison purposes, the unpromoted catalyst was also tested. Note that, a slight decrease of 0.68 $\% \cdot h^{-1}$ in the catalytic activity was observed for the unpromoted catalyst. This decrease in the catalytic activity over cobalt catalyst has been also observed by some authors [25]. Usually, the deactivation of the catalysts has been related to particle agglomeration or to the presence of nitrates species difficult to remove. However, the catalytic activity remained almost constant with an ammonia conversion close to 82 % at 400 ºC for 1K-Co/SiC catalyst due to the promoter effect of K metal, which could act as stabilizer of cobalt particles, which in turn, might enhance the stability of the catalyst [36,51].

The above results show that 1K-Co/SiC is a promising catalyst for the generation of CO_x-free hydrogen from ammonia decomposition.

4. Conclusion

Alkaline (K, Cs), alkaline-earth (Mg, Ca) and rare-earth (La, Ce) metals have been studied as promoters in Co/β-SiC (5 wt.%) catalysts for hydrogen production from ammonia decomposition reaction at low temperature. It has been seen that not all promoter metals improved the catalytic activity. Cs, despite its good properties, was not useful for this process due to the unfavourable effect over cobalt active sites. Mg and Ca promoted cobalt catalysts showed lower capacity for nitrogen desorption and higher cobalt particle size, respectively, which decreased the ammonia conversion. Ce promoted cobalt catalysts also presented decent properties but was inhibited by hydrogen.

Catalysts modified with K and La enhanced catalytic activity by means of the increase of the basicity and the modification of the electronic structure of cobalt active sites due to their suitable electron-donor properties. In addition, an increase in K loading above 1 wt.% was found to decrease the ammonia conversion by the partial blockage of the active sites by an excess of promoter metal. Therefore, 83 % of ammonia conversion is reached at low temperature (400 ºC) over 1K-Co/SiC over 24 h of reaction time, proving the excellent stability of the proposed catalyst.

5. Acknowledgments

This study was supported by the Regional Government of Castilla-La Mancha and the European Union [FEDER funds SBPLY/180501/000281].

6. References

[1] Z. Cesaro, M. Ives, R. Nayak-Luke, M. Mason, R. Bañares-Alcántara, Ammonia to power: Forecasting the levelized cost of electricity from green ammonia in large-scale power plants, Appl. Energy. 282 (2021). https://doi.org/10.1016/j.apenergy.2020.116009.

[2] Z. Abdin, A. Zafaranloo, A. Rafiee, W. Mérida, W. Lipiński, K.R. Khalilpour, Hydrogen as an energy vector, Renew. Sustain. Energy Rev. 120 (2020) 109620. https://doi.org/10.1016/j.rser.2019.109620.

[3] F.B. Juangsa, A.R. Irhamna, M. Aziz, Production of ammonia as potential hydrogen carrier: Review on thermochemical and electrochemical processes, Int. J. Hydrogen Energy. 46 (2021) 14455–14477. https://doi.org/10.1016/j.ijhydene.2021.01.214.

[4] G. Chehade, I. Dincer, Progress in green ammonia production as potential carbon-free fuel, Fuel. 299 (2021) 120845. https://doi.org/10.1016/j.fuel.2021.120845.

[5] Z. Wan, Y. Tao, J. Shao, Y. Zhang, H. You, Ammonia as an effective hydrogen carrier and a clean fuel for solid oxide fuel cells, Energy Convers. Manag. 228 (2021). https://doi.org/10.1016/j.enconman.2020.113729.

[6] N. Morlanés, S.P. Katikaneni, S.N. Paglieri, A. Harale, B. Solami, S.M. Sarathy, J. Gascon, A technological roadmap to the ammonia energy economy: Current state and missing technologies, Chem. Eng. J. 408 (2021) 127310. https://doi.org/10.1016/j.cej.2020.127310.

[7] B. Lee, J. Park, H. Lee, M. Byun, C.W. Yoon, H. Lim, Assessment of the economic potential: CO_x-free hydrogen production from renewables via ammonia decomposition for small-sized H_2 refueling stations, Renew. Sustain. Energy Rev. 113 (2019) 109262. https://doi.org/10.1016/j.rser.2019.109262.

[8] C. Smith, A.K. Hill, L. Torrente-Murciano, Current and future role of Haber-Bosch

ammonia in a carbon-free energy landscape, Energy Environ. Sci. 13 (2020) 331–344. https://doi.org/10.1039/c9ee02873k.
[9] S. Sittichompoo, H. Nozari, J.M. Herreros, N. Serhan, J.A.M. da Silva, A.P.E. York, P. Millington, A. Tsolakis, Exhaust energy recovery via catalytic ammonia decomposition to hydrogen for low carbon clean vehicles, Fuel. 285 (2021) 119111. https://doi.org/10.1016/j.fuel.2020.119111.
[10] V. Cechetto, L. Di Felice, J.A. Medrano, C. Makhloufi, J. Zuniga, F. Gallucci, H_2 production via ammonia decomposition in a catalytic membrane reactor, Fuel Process. Technol. 216 (2021) 106772. https://doi.org/10.1016/j.fuproc.2021.106772.
[11] I. Lucentini, X. Garcia, X. Vendrell, J. Llorca, Review of the Decomposition of Ammonia to Generate Hydrogen, Ind. Eng. Chem. Res. (2021) acs.iecr.1c00843. https://doi.org/10.1021/acs.iecr.1c00843.
[12] J. Jiang, Q. Dong, K. McCullough, J. Lauterbach, S. Li, M. Yu, Novel hollow fiber membrane reactor for high purity H_2 generation from thermal catalytic NH_3 decomposition, J. Memb. Sci. 629 (2021). https://doi.org/10.1016/j.memsci.2021.119281.
[13] M. Pinzón, A. Romero, A. de Lucas Consuegra, A.R. de la Osa, P. Sánchez, Hydrogen production by ammonia decomposition over ruthenium supported on SiC catalyst, J. Ind. Eng. Chem. 94 (2021) 326–335. https://doi.org/10.1016/j.jiec.2020.11.003.
[14] K.G. Kirste, K. McAulay, T.E. Bell, D. Stoian, S. Laassiri, A. Daisley, J.S.J. Hargreaves, K. Mathisen, L. Torrente-Murciano, CO_x-free hydrogen production from ammonia – mimicking the activity of Ru catalysts with unsupported Co-Re alloys, Appl. Catal. B Environ. 280 (2021) 119405. https://doi.org/10.1016/j.apcatb.2020.119405.
[15] I. Lucentini, G. García Colli, C.D. Luzi, I. Serrano, O.M. Martínez, J. Llorca, Catalytic ammonia decomposition over Ni-Ru supported on CeO_2 for hydrogen production: Effect of metal loading and kinetic analysis, Appl. Catal. B Environ. 286 (2021). https://doi.org/10.1016/j.apcatb.2021.119896.
[16] A.K. Hill, L. Torrente-Murciano, Low temperature H_2 production from ammonia using ruthenium-based catalysts: Synergetic effect of promoter and support, Appl. Catal. B Environ. 172–173 (2015) 129–135. https://doi.org/10.1016/j.apcatb.2015.02.011.
[17] S. Mukherjee, S. V. Devaguptapu, A. Sviripa, C.R.F. Lund, G. Wu, Low-temperature ammonia decomposition catalysts for hydrogen generation, Appl. Catal. B Environ. 226 (2018) 162–181. https://doi.org/10.1016/j.apcatb.2017.12.039.
[18] T.E. Bell, L. Torrente-Murciano, H_2 Production via Ammonia Decomposition Using Non-Noble Metal Catalysts: A Review, Top. Catal. 59 (2016) 1438–1457. https://doi.org/10.1007/s11244-016-0653-4.
[19] E. García-Bordejé, S. Armenise, L. Roldán, Toward Practical Application Of H_2 Generation From Ammonia Decomposition Guided by Rational Catalyst Design, Catal. Rev. 56 (2014) 220–237. https://doi.org/10.1080/01614940.2014.903637.
[20] A.R. de la Osa, A. Romero, J. Díez-Ramírez, J.L. Valverde, P. Sánchez, Influence of a Zeolite-Based Cascade Layer on Fischer–Tropsch Fuels Production over Silicon Carbide Supported Cobalt Catalyst, Top. Catal. 60 (2017) 1082–1093. https://doi.org/10.1007/s11244-017-0792-2.
[21] J.M. García-Vargas, J.L. Valverde, J. Díez, P. Sánchez, F. Dorado, Influence of alkaline and alkaline-earth cocations on the performance of Ni/β-SiC catalysts in the methane tri-reforming reaction, Appl. Catal. B Environ. 148–149 (2014) 322–

329. https://doi.org/10.1016/j.apcatb.2013.11.013.
[22] J. Díez-Ramírez, J.A. Díaz, P. Sánchez, F. Dorado, Optimization of the Pd/Cu ratio in Pd-Cu-Zn/SiC catalysts for the CO_2 hydrogenation to methanol at atmospheric pressure, J. CO_2 Util. 22 (2017) 71–80. https://doi.org/10.1016/j.jcou.2017.09.012.
[23] X.-C. Hu, W.-W. Wang, Z. Jin, X. Wang, R. Si, C.-J. Jia, Transition metal nanoparticles supported La-promoted MgO as catalysts for hydrogen production via catalytic decomposition of ammonia, J. Energy Chem. 38 (2019) 41–49. https://doi.org/10.1016/j.jechem.2018.12.024.
[24] Y.Q. Gu, Z. Jin, H. Zhang, R.J. Xu, M.J. Zheng, Y.M. Guo, Q.S. Song, C.J. Jia, Transition metal nanoparticles dispersed in an alumina matrix as active and stable catalysts for CO_x-free hydrogen production from ammonia, J. Mater. Chem. A. 3 (2015) 17172–17180. https://doi.org/10.1039/c5ta04179a.
[25] Y. Xun, X. He, H. Yan, Z. Gao, Z. Jin, C. Jia, Fe- and Co-doped lanthanum oxides catalysts for ammonia decomposition: Structure and catalytic performances, J. Rare Earths. 35 (2017) 15–23. https://doi.org/10.1016/S1002-0721(16)60167-9.
[26] Y. Im, H. Muroyama, T. Matsui, K. Eguchi, Ammonia decomposition over nickel catalysts supported on alkaline earth metal aluminate for H_2 production, Int. J. Hydrogen Energy. 45 (2020) 26979–26988. https://doi.org/10.1016/j.ijhydene.2020.07.014.
[27] Z. Zhao, H. Zou, W. Lin, Effect of rare earth and other cationic promoters on properties of $CoMoN_x$/CNTs catalysts for ammonia decomposition, J. Rare Earths. 31 (2013) 247–250. https://doi.org/10.1016/S1002-0721(12)60266-X.
[28] J. Díez-Ramírez, P. Sánchez, V. Kyriakou, S. Zafeiratos, G.E. Marnellos, M. Konsolakis, F. Dorado, Effect of support nature on the cobalt-catalyzed CO_2 hydrogenation, J. CO_2 Util. 21 (2017) 562–571. https://doi.org/10.1016/j.jcou.2017.08.019.
[29] S. Armenise, E. García-Bordejé, J.L. Valverde, E. Romeo, A. Monzón, A Langmuir–Hinshelwood approach to the kinetic modelling of catalytic ammonia decomposition in an integral reactor, Phys. Chem. Chem. Phys. 15 (2013) 12104. https://doi.org/10.1039/c3cp50715g.
[30] S. Armenise, F. Cazaña, A. Monzón, E. García-Bordejé, In situ generation of CO_x-free H_2 by catalytic ammonia decomposition over Ru-Al-monoliths, Fuel. 233 (2018) 851–859. https://doi.org/10.1016/j.fuel.2018.06.129.
[31] C. Huang, Y. Yu, X. Tang, Z. Liu, J. Zhang, C. Ye, Y. Ye, R. Zhang, Hydrogen generation by ammonia decomposition over Co/CeO_2 catalyst: Influence of support morphologies, Appl. Surf. Sci. 532 (2020) 147335. https://doi.org/10.1016/j.apsusc.2020.147335.
[32] J.M. García-Vargas, J.L. Valverde, J. Díez, P. Sánchez, F. Dorado, Preparation of Ni-Mg/β-SiC catalysts for the methane tri-reforming: Effect of the order of metal impregnation, Appl. Catal. B Environ. 164 (2015) 316–323. https://doi.org/10.1016/j.apcatb.2014.09.044.
[33] M. Thommes, K. Kaneko, A. V. Neimark, J.P. Olivier, F. Rodriguez-Reinoso, J. Rouquerol, K.S.W. Sing, Physisorption of gases, with special reference to the evaluation of surface area and pore size distribution (IUPAC Technical Report), Pure Appl. Chem. 87 (2015) 1051–1069. https://doi.org/10.1515/pac-2014-1117.
[34] S. Li, A. Li, S. Krishnamoorthy, E. Iglesia, Effects of Zn, Cu, and K promoters on the structure and on the reduction, carburization, and catalytic behavior of iron-based Fischer-Tropsch synthesis catalysts, Catal. Letters. 77 (2001) 197–205. https://doi.org/10.1023/A:1013284217689.
[35] A.R. de la Osa, A. De Lucas, J. Díaz-Maroto, A. Romero, J.L. Valverde, P. Sánchez., FTS fuels production over different Co/SiC catalysts, Catal. Today. 187

(2012) 173–182. https://doi.org/10.1016/j.cattod.2011.12.029.
[36] S.J. Wang, S.F. Yin, L. Li, B.Q. Xu, C.F. Ng, C.T. Au, Investigation on modification of Ru/CNTs catalyst for the generation of CO_x-free hydrogen from ammonia, Appl. Catal. B Environ. 52 (2004) 287–299. https://doi.org/10.1016/j.apcatb.2004.05.002.
[37] A.R. De La Osa, A. De Lucas, J.L. Valverde, A. Romero, I. Monteagudo, P. Coca, P. Sánchez, Influence of alkali promoters on synthetic diesel production over Co catalyst, Catal. Today. 167 (2011) 96–106. https://doi.org/10.1016/j.cattod.2010.11.064.
[38] H. Zhang, Y.A. Alhamed, W. Chu, Z. Ye, A. Alzahrani, L. Petrov, Controlling Co-support interaction in Co/MWCNTs catalysts and catalytic performance for hydrogen production via NH_3 decomposition, Appl. Catal. A Gen. 464–465 (2013) 156–164. https://doi.org/10.1016/j.apcata.2013.05.046.
[39] K. Okura, T. Okanishi, H. Muroyama, T. Matsui, K. Eguchi, Promotion effect of rare-earth elements on the catalytic decomposition of ammonia over Ni/Al_2O_3 catalyst, Appl. Catal. A Gen. 505 (2015) 77–85. https://doi.org/10.1016/j.apcata.2015.07.020.
[40] W.F. Lim, K.Y. Cheong, Effects of post-deposition annealing temperature on metal-organic decomposed lanthanum cerium oxide film as metal reactive oxide layer on 4H-SiC, Mater. Chem. Phys. 140 (2013) 622–633. https://doi.org/10.1016/J.MATCHEMPHYS.2013.04.016.
[41] A.R. De La Osa, A. De Lucas, A. Romero, J.L. Valverde, P. Sánchez, Fischer-Tropsch diesel production over calcium-promoted Co/alumina catalyst: Effect of reaction conditions, Fuel. 90 (2011) 1935–1945. https://doi.org/10.1016/j.fuel.2010.12.024.
[42] L. Torrente-Murciano, A.K. Hill, T.E. Bell, Ammonia decomposition over cobalt/carbon catalysts—Effect of carbon support and electron donating promoter on activity, Catal. Today. 286 (2017) 131–140. https://doi.org/10.1016/j.cattod.2016.05.041.
[43] S. Podila, Y.A. Alhamed, A.A. Alzahrani, L.A. Petrov, Hydrogen production by ammonia decomposition using Co catalyst supported on Mg mixed oxide systems, Int. J. Hydrogen Energy. 40 (2015) 15411–15422. https://doi.org/10.1016/j.ijhydene.2015.09.057.
[44] J.A. Díaz, M. Calvo-Serrano, A.R. De La Osa, A.M. García-Minguillán, A. Romero, A. Giroir-Fendler, J.L. Valverde, β-Silicon carbide as a catalyst support in the fischer-tropsch synthesis: Influence of the modification of the support by a pore agent and acidic treatment, Appl. Catal. A Gen. 475 (2014) 82–89. https://doi.org/10.1016/j.apcata.2014.01.021.
[45] K. Shimura, T. Miyazawa, T. Hanaoka, S. Hirata, Fischer-Tropsch synthesis over alumina supported cobalt catalyst: Effect of promoter addition, Appl. Catal. A Gen. 494 (2015) 1–11. https://doi.org/10.1016/j.apcata.2015.01.017.
[46] R.A. Iloy, K. Jalama, Effect of operating temperature, pressure and potassium loading on the performance of silica-supported Cobalt catalyst in CO_2 hydrogenation to hydrocarbon fuel, Catalysts. 9 (2019) 807. https://doi.org/10.3390/catal9100807.
[47] J. Sun, Q. Feng, Q. Liu, S. Ji, Y. Fang, X. Peng, Z.J. Wang, An Al_2O_3-Coated SiC-Supported Ni Catalyst with Enhanced Activity and Improved Stability for Production of Synthetic Natural Gas, Ind. Eng. Chem. Res. 57 (2018) 14899–14909. https://doi.org/10.1021/acs.iecr.8b02103.
[48] J.M. García-Vargas, J.L. Valverde, A. de Lucas-Consuegra, B. Gómez-Monedero, P. Sánchez, F. Dorado, Precursor influence and catalytic behaviour of Ni/CeO_2 and

Ni/SiC catalysts for the tri-reforming process, Appl. Catal. A Gen. 431–432 (2012) 49–56. https://doi.org/10.1016/j.apcata.2012.04.016.
[49] J.M. García-Vargas, J.L. Valverde, F. Dorado, P. Sánchez, Influence of the support on the catalytic behaviour of Ni catalysts for the dry reforming reaction and the tri-reforming process, J. Mol. Catal. A Chem. 395 (2014) 108–116. https://doi.org/10.1016/j.molcata.2014.08.019.
[50] Ł. Czekajło, Z. Lendzion-Bieluń, Effect of preparation conditions and promoters on the structure and activity of the ammonia decomposition reaction catalyst based on nanocrystalline cobalt, Chem. Eng. J. 289 (2016) 254–260. https://doi.org/10.1016/j.cej.2015.12.093.
[51] T. Kocer, F.E.S. Oztuna, S.F. Kurtoğlu, U. Unal, A. Uzun, Graphene aerogel-supported ruthenium nanoparticles for CO_x-free hydrogen production from ammonia, Appl. Catal. A Gen. 610 (2021). https://doi.org/10.1016/j.apcata.2020.117969.
[52] K. Okura, T. Okanishi, H. Muroyama, T. Matsui, K. Eguchi, Additive effect of alkaline earth metals on ammonia decomposition reaction over Ni/Y_2O_3 catalysts, RSC Adv. 6 (2016) 85142–85148. https://doi.org/10.1039/c6ra19005g.
[53] S. Podila, H. Driss, S.F. Zaman, Y.A. Alhamed, A.A. Alzahrani, M.A. Daous, L.A. Petrov, Hydrogen generation by ammonia decomposition using $Co/MgO\text{-}La_2O_3$ catalyst: Influence of support calcination atmosphere, J. Mol. Catal. A Chem. 414 (2016) 130–139. https://doi.org/10.1016/j.molcata.2016.01.012.
[54] K. Okura, T. Okanishi, H. Muroyama, T. Matsui, K. Eguchi, Ammonia Decomposition over Nickel Catalysts Supported on Rare-Earth Oxides for the On-Site Generation of Hydrogen, ChemCatChem. 8 (2016) 2988–2995. https://doi.org/10.1002/cctc.201600610.
[55] M. Pinzón, E. Ruiz-López, A. Romero, A.R. de la Osa, P. Sánchez, A. de Lucas-Consuegra, Electrochemical activation of Ru catalyst with alkaline ion conductors for the catalytic decomposition of ammonia, Mol. Catal. 511 (2021) 111721. https://doi.org/10.1016/j.mcat.2021.111721.
[56] Z.-S. Zhang, X.-P. Fu, W.-W. Wang, Z. Jin, Q.-S. Song, C.-J. Jia, Promoted porous $Co_3O_4\text{-}Al_2O_3$ catalysts for ammonia decomposition, Sci. China Chem. 61 (2018) 1389–1398. https://doi.org/10.1007/s11426-018-9261-5.
[57] T.E. Bell, H. Ménard, J.-M. González Carballo, R. Tooze, L. Torrente-Murciano, Hydrogen production from ammonia decomposition using $Co/\gamma\text{-}Al_2O_3$ catalysts – Insights into the effect of synthetic method, Int. J. Hydrogen Energy. 45 (2020) 27210–27220. https://doi.org/10.1016/j.ijhydene.2020.07.090.
[58] S.F. Yin, B.Q. Xu, X.P. Zhou, C.T. Au, A mini-review on ammonia decomposition catalysts for on-site generation of hydrogen for fuel cell applications, Appl. Catal. A Gen. 277 (2004) 1–9. https://doi.org/10.1016/j.apcata.2004.09.020.
[59] S.F. Yin, Q.H. Zhang, B.Q. Xu, W.X. Zhu, C.F. Ng, C.T. Au, Investigation on the catalysis of CO_x-free hydrogen generation from ammonia, J. Catal. 224 (2004) 384–396. https://doi.org/10.1016/j.jcat.2004.03.008.
[60] K. Tamai, S. Hosokawa, H. Asakura, K. Teramura, T. Tanaka, Low-temperature NO_x trapping on alkali or alkaline earth metal modified TiO_2 photocatalyst, Catal. Today. 332 (2019) 76–82. https://doi.org/10.1016/J.CATTOD.2018.07.045.
[61] K. Asano, C. Ohnishi, S. Iwamoto, Y. Shioya, M. Inoue, Potassium-doped Co_3O_4 catalyst for direct decomposition of N_2O, Appl. Catal. B Environ. 78 (2008) 242–249. https://doi.org/10.1016/j.apcatb.2007.09.016.
[62] Z. Wang, Z. Cai, Z. Wei, Highly Active Ruthenium Catalyst Supported on Barium Hexaaluminate for Ammonia Decomposition to CO_x-Free Hydrogen, ACS Sustain. Chem. Eng. 7 (2019) 8226–8235.

https://doi.org/10.1021/acssuschemeng.8b06308.
[63] A. Klegova, A. Inayat, P. Indyka, J. Gryboś, Z. Sojka, K. Pacultová, W. Schwieger, A. Volodarskaja, P. Kuśtrowski, A. Rokicińska, D. Fridrichová, L. Obalová, Cobalt mixed oxides deposited on the SiC open-cell foams for nitrous oxide decomposition, Appl. Catal. B Environ. 255 (2019) 117745. https://doi.org/10.1016/j.apcatb.2019.117745.
[64] L. Gavrilović, J. Save, E.A. Blekkan, The effect of potassium on cobalt-based Fischer-Tropsch catalysts with different cobalt particle sizes, Catalysts. 9 (2019) 351. https://doi.org/10.3390/catal9040351.
[65] G.E. Pitselis, P.D. Petrolekas, C.G. Vayenas, Electrochemical promotion of ammonia decomposition over Fe catalyst films interfaced with K^+- & H^+-conductors, Ionics (Kiel). 3 (1997) 110–116. https://doi.org/10.1007/BF02375532.
[66] H.A. Lara-García, J.A. Mendoza-Nieto, H. Pfeiffer, L. Torrente-Murciano, CO_x-free hydrogen production from ammonia on novel cobalt catalysts supported on 1D titanate nanotubes, Int. J. Hydrogen Energy. 44 (2019) 30062–30074. https://doi.org/10.1016/j.ijhydene.2019.09.120.